Abstracta

Ano XXVII - N. 01

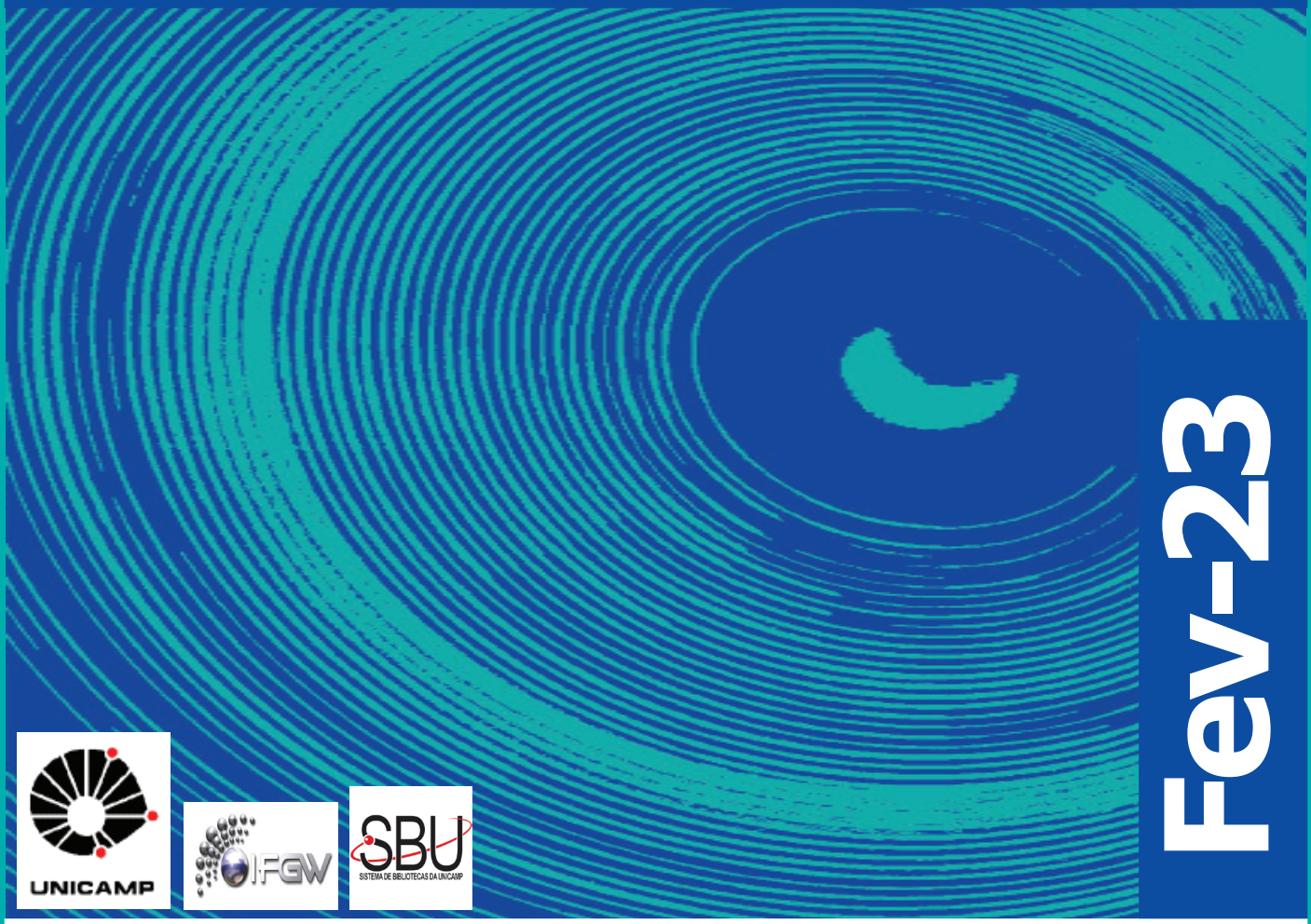

Fev-23

Artigos publicados 2022 - P307-2022 à P337-2022

Eventos publicados 2022 - P338-2022

Material editorial 2022 - M002-2022

Artigos publicados 2023 - P001-2023 à P008-2023

Defesas de Dissertações do IFGW - D001-2023

Defesas de Teses do IFGW - T001-2023 à T002-2023

Artigos publicados 2022

[P307-2022] "Characterizing the initial conditions of heavy--ion collisions at the LHC with mean transverse momentum and anisotropic flow correlations"

Acharya, S.; Adamova, D.; **Chinellato, D. D.*; Guardiano, G. G.*; Jahnke, C.*; Takahashi, J.***; et al. ALICE Collaboration

Correlations between mean transverse momentum [P-T] and anisotropic flow coefficients v(2) or v(3) are measured as a function of centrality in Pb-Pb and Xe-Xe collisions at root(NN)--N-s = 5.02 TeV and 5.44 TeV, respectively, with ALICE. In addition, the recently proposed higher-order correlation between [P-T], v(2), and v(3) is measured for the first time, which shows an anticorrelation for the presented centrality ranges. These measurements are compared with hydrodynamic calculations using IP-Glasma and T(R)ENTo initial-state shapes, the former based on the Color Glass Condensate effective theory with gluon saturation, and the latter a parameterized model with nucleons as the relevant degrees of freedom. The data are better described by the IP-Glasma rather than the T(R) ENTo based calculations. In particular, Trajectum and JETSCAPE predictions, both based on the T(R)ENTo initial state model but with different parameter settings, fail to describe the measurements. As the correlations between [P-T] and v(n) are mainly driven by the correlations of the size and the shape of the system in the initial state, these new studies pave a novel way to characterize the initial state and help pin down the uncertainty of the extracted properties of the quark--gluon plasma recreated in relativistic heavy-ion collisions.

PHYSICS LETTERS B 834, 137393, 2022. DOI: 10.1016/j.physletb.2022.137393

[P308-2022] "Chirality-assisted spin Hall effect of light in the vicinity of the quasi-antidual symmetry mode of a chiral sphere"

Ali, R.*

The spin Hall shift (SHS) refers to a transverse shift in the scattering plane during the spin-orbit interaction (SOI). SHS is considerably small when light is scattered by a sphere due to the absence of unidirectional scattering. This work shows that the chiral property of a sphere can offer a platform to optimize the SOI by achieving nearly zero forward scattering with significant backward scattering. As a result, a polarization transformation takes place and the scattered field transfers its maximum spin angular momentum to orbital angular momentum. Consequently, an enhanced transversal shift is observed due to the momentum conservation of the scattered field. The results reveal that the shift strongly depends on the handedness of the chiral sphere and the helicity of the incident beam. Thus, offering an alternative paradigm for the quantitative measurement of chirality parameters of a single chiral nanoparticle. We hope that these results will potentially shed new light on the SOI of various forms that can find potential applications such as optical sensing, chiral resolution of single nanoparticles, precision measurements, and the manipulation of subwavelength nanoparticles.

PHYSICAL REVIEW A 106[6], 063508, 2022. DOI: 10.1103/PhysRevA.106.063508

[P309-2022] "Colorimetric Detection of SARS-CoV-2 Using Plasmonic Biosensors and Smartphones"

Materon, E. M.; Gomez, F. R.; Almeida, M. B.; **Shimizu, F. M.***; Wong, A.; Teodoro, K. B. R.; Silva, F. S. R.; Lima, M. J. A.; Angelim, M. K. S. C.; Melendez, M. E.; Porras, N.; Vieira, P. M.; Correa, D. S.; Carrilho, E.; Oliveira Jr., O. N.; Azevedo, R. B.; Goncalves, D.

Low-cost, instrument-free colorimetric tests were developed to detect SARS-CoV-2 using plasmonic biosensors with Au nanoparticles functionalized with polyclonal antibodies (f-AuNPs). Intense color changes were noted with the naked eye owing to plasmon coupling when f-AuNPs form clusters on the virus, with high sensitivity and a detection limit of 0.28 PFU mL(-1) (PFU stands for plaque-forming units) in human saliva. Plasmon coupling was corroborated with computer simulations using the finite-difference time-domain (FDTD) method. The strategies based on preparing plasmonic biosensors with f-AuNPs are robust to permit SARS-CoV-2 detection via dynamic light scattering and UV-vis spectroscopy without interference from other viruses, such as influenza and dengue viruses. The diagnosis was made with a smartphone app after processing the images collected from the smartphone camera, measuring the concentration of SARS-CoV-2. Both image processing and machine learning algorithms were found to provide COVID-19 diagnosis with 100% accuracy for saliva samples. In subsidiary experiments, we observed that the biosensor could be used to detect the virus in river waters without pretreatment. With fast responses and requiring small sample amounts (only 20 mu L), these colorimetric tests can be deployed in any location within the point-of-care diagnosis paradigm for epidemiological control. The extensive production of coal fly ash by coal combustion is an issue of concern due to its environmental impact. TiO2-zeolite composites were synthesized, at low cost, using recycled coal fly ash from a local thermoelectric power plant to produce the zeolite using the hydrothermal method. TiO2 was loaded by means of the impregnation method using ethanol and titanium isopropoxide between 8.7 and 49.45 wt% TiO2. The samples were characterized by X-ray diffraction, Raman, electron spin resonance, high-resolution transmission electron microscopy, N-2 adsorption-desorption, doppler broadening of annihilation radiation, and diffuse reflectance techniques, and the photocatalytic activity of the composites was evaluated according to the degradation of methyl orange under UV light. The results show that TiO2 crystallizes in the anatase phase with a Ti3+ oxidation state, without post-treatment. TiO2 particles were located within the pores of the substrate and on its surface, increasing the surface area of the composites in comparison with that of the substrates. Samples with TiO2 at 8.7 and 25 wt% immobilized on hydroxysodalite show the highest degradation of methyl orange among all studied materials, including the commercial TiO2 Degussa P25 under UV light.

CONDENSED MATTER 7[4], 69, 2022. DOI: 10.3390/condmat7040069

[P310-2022] "Dark Energy Survey year 3 results: Constraints on cosmological parameters and galaxy-bias models from galaxy clustering and galaxy-galaxy lensing using the redMaGiC sample"

Pandey, S.; Krause, E.; **Navarro-Alsina, A.***; et al. DES Collaboration

We constrain cosmological parameters and galaxy-bias parameters using the combination of galaxy clustering and galaxy-galaxy lensing measurements from the Dark Energy Survey (DES) year-3 data. We describe our modeling framework and choice of scales analyzed, validating their robustness to theoretical uncertainties in small-scale clustering by analyzing simulated data. Using a linear galaxy-bias model and redMaGiC galaxy sample, we obtain 10% constraints on the matter density of the Universe. We also implement a nonlinear galaxy-bias model to probe smaller scales that includes parametrization based on hybrid perturbation theory and find that it leads to a 17% gain in cosmological constraining power. We perform robustness tests of our methodology pipeline and demonstrate stability of the constraints to changes in the theory model. Using the redMaGiC galaxy sample as foreground lens galaxies and adopting the best-fitting cosmological parameters from DES year-1 data, we find the galaxy clustering and galaxygalaxy lensing measurements to exhibit significant signals akin to decorrelation

between galaxies and mass on large scales, which is not expected in any current models. This likely systematic measurement error biases our constraints on galaxy bias and the S-8 parameter. We find that a scale-, redshift- and sky-areaindependent phenomenological decorrelation parameter can effectively capture this inconsistency between the galaxy clustering and galaxy-galaxy lensing. We trace the source of this correlation to a colordependent photometric issue and minimize its impact on our result by changing the selection criteria of redMaGiC galaxies. Using this new sample, our constraints on the S-8 parameter are consistent with previous studies and we find a small shift in the Omega(m). constraints compared to the fiducial redMaGiC sample. We infer the constraints on the mean host-halo mass of the redMaGiC galaxies in this new sample from the large-scale bias constraints, finding the galaxies occupy halos of mass approximately 1.6 x 10(13) M-circle dot/h.

PHYSICAL REVIEW D 106[4], 043520, 2022. DOI: 10.1103/PhysRevD.106.043520

[P311-2022] "Dirac dark matter, neutrino masses, and dark baryogenesis"

Restrepo, D.*; Rivera, A.; Tangarife, W.

We present a gauged baryon number model as an example of models where all new fermions required to cancel out the anomalies help to solve phenomenological problems of the standard model (SM). Dark fermion doublets, along with the isosinglet charged fermions, in conjunction with a set of SM--singlet fermions, participate in the generation of small neutrino masses through the Dirac-dark Zee mechanism. The other SM-singlets explain the dark matter in the Universe, while their coupling to an inert singlet scalar is the source of the CP violation. In the presence of a strong first-order electroweak phase transition, this "dark" CP violation allows for a successful electroweak baryogenesis mechanism.

PHYSICAL REVIEW D 106[5], 055021, 2022. DOI: 10.1103/PhysRevD.106.055021

[P312-2022] "Dislocation-position fluctuations in solid He-4 as collective variables in a quantum crystal"

Koning, M. de*; Cai, W.

Quantum behavior at mesoscopic length scales is of significant interest, both from a fundamental-physics standpoint, as well as in the context of technological advances. In this light, the description of collective variables comprising large numbers of atoms, but nevertheless displaying non-classical behavior, is a fundamental problem. Here, we show that an effective--Hamiltonian approach for such variables, as has been applied to describe the quantum behavior of coupled qubit/oscillator systems, can also be very useful in understanding intrinsic behavior of quantum materials. We consider lattice dislocations - naturally occurring mesoscopic line defects in crystals - in the prototypical bosonic quantum crystal, solid He-4. For this purpose, we map fully atomistic quantum simulations onto effective one-dimensional Hamiltonians in which the collective dislocation-position variables are represented as interacting, massive quantum particles. The results provide quantitative understanding of several experimental observations in solid He-4.

NPJ QUANTUM MATERIALS 7[1], 119, 2022. DOI: 10.1038/s41535-022-00533-8

[P313-2022] "Electron tracks simulation in water: Performance comparison between GPU CPU and the EUMED grid installation"

Seif, E.; El Bitar, Z.; Incerti, S.; **Bernal, M. A.***; Francis, Z.

Purpose: We explored different technologies to minimize simulation time of the Monte-Carlo method for track generation following the Geant4-DNA processes for electrons in water. Methods: A GPU software tool is developed for electron track simulations. A similar CPU version is also developed using the same collision models. CPU simulations were carried out on a single user desktop computer and on the computing grid France Grilles using 10 and 100 computing nodes. Computing time results for CPU, GPU, and grid simulations are compared with those using Geant4-DNA processes.Results: The CPU simulations better performs when the number of electrons is less than 104 with 100 eV initial energy, this number decreases as the energy increases. The GPU simulations gives better results when the number of electrons is more than 104 with initial energy of 100 eV, this number decreases to 103 for electrons with 10KeV and increases back with higher energy. The use of the grid introduces an additional queuing time which slows down the overall simulation performance. Thus, the Grid gives better performance when the number of electrons is over 105 with initial energy of 10KeV, and this number decreases as the energy increases.Conclusions: The CPU is best suited for small numbers of primary incident electrons. The GPU is best suited when the number of primary incident particles occupies sufficient resources on GPU card in order to get an important computing power. The grid is best suited for simulations with high number of primary incident electrons with high initial energy.

PHYSICA MEDICA-EUROPEAN JOURNAL OF MEDICAL PHYSICS 104, 56-66, 2022. DOI: 10.1016/j.ejmp.2022.10.020

[P314-2022] "Ethanol Oxidation Reaction Mechanism on Gold Nanowires from Density Functional Theory"

Bueno, O. V. M.*; San-Miguel, M. A.; **Silva, E. Z. da***

Thin gold nanowires (NWs) are materials that could be used as support in different chemical reactions. Using density functional theory (DFT) it was shown that NWs that form linear atomic chains (LACs) are suitable for stimulating chemical reactions. To this end, the oxidation reaction of ethanol supported on the LACs of Au-NWs was investigated. Two types of LACs were used for the study, one pure and the other with an oxygen impurity. The results showed that the oxygen atom in the LAC fulfills important functions throughout the reaction pathway. Before the chemical reaction, it was observed that the LAC with impurity gains structural stability, that is, the oxygen acts as an anchor for the gold atoms in the LAC. In addition, the LAC was shown to be sensitive to disturbances in its vicinity, which modifies its nucleophilic character. During the chemical reaction, the oxidation of ethanol occurs through two different reaction paths and in two stages, both producing acetaldehyde (CH3CHO). The different reaction pathways are a consequence of the presence of oxygen in the LAC (oxygen conditions the formation of reaction intermediates). In addition, the oxygen in the LAC also modifies the kinetic behavior in both reaction stages. It was observed that, by introducing an oxygen impurity in the LAC, the activation energy barriers decrease similar to 69 % and similar to 97 % in the first and second reaction stages, respectively.

CHEMPHYSCHEM, e202200, 2022. DOI: 10.1002/cphc.202200723

[P315-2022] "Evidence for WW/WZ vector boson scattering in the decay channel l nu qq produced in association with two jets in proton-proton collisions at root s=13TeV"

Tumasyan, A.; Adam, W.; **Chinellato, J. A.***; et al. CMS Collaboration

Evidence is reported for electroweak (EW) vector boson scattering in the decay channel l nu qq of two weak vector bosons WV(V = Wor Z), produced in association with two parton jets. The search uses a data set of proton-proton collisions at 13TeVcollected with the CMS detector during 2016-2018 with an integrated luminosity of 138fb(-1). Events are selected requiring one lepton (electron or muon), moderate missing transverse momentum, two jets with a large pseudorapidity separation and a large dijet invariant mass, and a signature consistent with the hadronic decay of a W/Zboson. The cross section is computed in a fiducial phase space defined at parton level requiring all parton transverse momenta p(T)> 10 GeVand at least one pair of outgoing partons with invariant mass mqq> 100 GeV. The measured and expected EW WV-production cross sections are 1.90(-0.46)(+0.5)3 pb and 2.23(-0.11)(+0.08)(scale) +/- 0.05(PDF) pb, respectively, where PDF is the parton distribution function. The observed EW signal strength is mu EW= 0.85 +/- 0.12 (stat)(-0.17)(+0.19)(syst), corresponding to a signal significance of 4.4 standard deviations with 5.1 expected, and it is measured keeping the quantum chromodynamics (QCD) associated diboson production fixed to the standard model prediction. This is the first evidence of vector boson scattering in the l nu qq decay channel at LHC. The simultaneous measurement of the EW and QCD associated diboson production agrees with the standard model prediction.

PHYSICS LETTERS B 834, 137438, 2022. DOI: 10.1016/j.physletb.2022.137438

[P316-2022] "Evolution of the Fe-Co magnetism and magnetic proximity effects in alternate Fe/Co monolayers on nonmagnetic Cu3Au(001)"

Cabral, L.*; Macedo, W. A. A.; **Silva, E. Z. da***

Magnetic heterostructures with ferromagnetic/nonmagmetic interfaces are very interesting materials due to the possibility to switch the magnetization, to control the induced magnetic moment, and also due to interfacial effects. The tuning of the spin-orbit coupling in magnetic materials allows engineering new spintronic devices. Using density functional theory, the induced local magnetic moments in copper and gold surface atoms of Cu3Au(001) due to the deposited alternate magnetic Fe and Co monolayers were studied. To observe the tuning mechanism, the spin density of the FeCo/Cu3Au(001) as a function of the number of deposited magnetic monolayers was extensively investigated. The Fe/Co deposition induces a hybridization between electronic states of the magnetic and nonmagnetic interface atoms, generating a broadening in d bands of the deposited material, engineering the magnetic moments of the interface atoms. This observed hybridization elucidates the charge variation in the interface atoms for stacking sequences starting with Fe or with Co as the first magnetic layer in direct contact with the Cu3Au(001) substrate. By performing the spin-charge density calculations, we demonstrated that this magnetic induction occurs only for the nonmagnetic Cu-Au atoms at the Cu3Au(001) surface.

PHYSICAL REVIEW B 106[21], 214430, 2022. DOI: 10.1103/PhysRevB.106.214430

[P317-2022] "Failure of the geometric approach prediction of excess work scaling for open and isolated quantum systems"

Soriani, A.*; Miranda, E.*; Bonanca, M. V. S.*

The task of finding optimal protocols that minimize the energetic cost of thermodynamic processes of long yet finite duration tau is a pressing one. We approach this problem here in a rigorous and systematic fashion by means of the adiabatic perturbation theory of closed Hamiltonian quantum systems. Our main finding is a 1/tau (2) scaling of the excess work for large tau in gapped systems. This result is at odds with the asymptotic 1/tau prediction of the geometric approach to optimization, which is predicated on the slow evolution of open systems close to canonical equilibrium. In contrast, our approach does not lead to an obvious geometric interpretation. Furthermore, as the thermodynamic work does not depend on how an isolated quantum system is split into a system of interest and its environment, our results imply the failure of the geometric approach prediction even for open systems. Additionally, we provide alternative optimization procedures, both for slowly--varying processes described by adiabatic perturbation theory and for weakly-varying processes described by linear response theory. Our findings are benchmarked and confirmed through the application to the driven transverse-field Ising chain.

NEW JOURNAL OF PHYSICS 24[11], 113037, 2022. DOI: 10.1088/1367-2630/aca177

[P318-2022] "Kaon production in high multiplicity events at the Large Hadron Collider"

Lima, Y. N.; **Giannini, A. V.***; Goncalves, V. P.

The production of the KS0 meson in high multiplicity pp collisions at root s = 13 TeV is investigated considering the hybrid formalism and the solution of the running coupling Balitsky-Kovchegov (BK) equation. The associated cross section is estimated and compared with the experimental data for the transverse momentum spectrum. Moreover, we analyze the self-normalized yields of KS0 mesons as a function of the multiplicity of coproduced charged hadrons and demonstrate that a steep increasing is theoretically predicted. A comparison with the ALICE data is presented considering two distinct solutions of the BK equation.

PHYSICAL REVIEW C 106[6], 065206, 2022. DOI: 10.1103/PhysRevC.106.065206

[P319-2022] "Magnetic interactions of 4f electrons in the topological insulator chalcogenide Bi2Se3"

Souza, J. C.*; Carlone, M.; Lesseux, G. G.; **Pizzi, H. B.*; Freitas, G. S.*; Urbano, R. R.***; Venegas, A.; **Pagliuso, P. G.***

The gap-opening mechanism of a topological insulator, the quantum anomalous Hall effect, and the axion physics are still pressing open questions, and a microscopic viewpoint to further understand the role of magnetism in topology is highly desirable. In this work we have performed a microscopic investigation, by means of electron spin resonance (ESR) along with complementary bulk measurements, on the chalcogenide (Bi1--xGdx)2Se3 (x = 0, 0.001, 0.002 and 0.006). Our analysis of the Gd3+ spin dynamics reveals no significant change of the Fermi surface as a function of Gd3+ concentration, which indicates that the 4 f magnetism is different from the nonlocal effects induced by transition metal (d electrons) substitutions. Additionally, we observe an unusual evolution of the Gd3+ ESR spectra as a function of the applied magnetic field, which we discuss considering the magnetic interaction between Gd3+ 4 f electrons and impurity centers such as Se vacancies. This interaction would give rise to a local weak antilocalization effect surrounding the Gd3+ ions. Such a mechanism is observable due to particular details of the Gd3+ 4 f electrons' magnetism in this system compared to that of d electrons. Our work points out that rare-earth substitutions in this model topological insulator are a promising path to explore the axion insulating systems.

PHYSICAL REVIEW B 106[23], 235109, 2022. DOI: 10.1103/PhysRevB.106.235109

[P320-2022] "Measurement of the pi(-)-Ar total hadronic cross section at the LArIAT experiment"

Gramellini, E.; Ho, J.; **Dedin, P.*; Gratieri, D. R.*; Kemp, E.*; Machado, A. A. B.*; Santos, L. M.*; Gelli, B. P.*; Guzzo, M. R.*; Segreto, E.*; Soares Nunes, M.***; et al. LArIAT Collaboration

We present the first measurement of the negative pion total hadronic cross section on argon in a restricted phase space, which we performed at the Liquid Argon In ATestbeam (LArIAT) experiment. All hadronic reaction channels, as well as hadronic elastic interactions with scattering angle greater than 5 degrees are included. The pions have kinetic energies in the range 100-700 MeVand are produced by a beam of charged particles impinging on a solid target at the Fermilab test beam facility. LArIAT employs a 0.24 ton active mass liquid argon time projection chamber (LArTPC) to measure the pion hadronic interactions. For this measurement, LArIAT has developed the "thin slice method," a new technique to measure cross sections with LArTPCs. While moderately higher, our measurement of the pi(-)-Ar total hadronic cross section is generally in agreement with the GEANT4 prediction.

PHYSICAL REVIEW D 106[5], 052009, 2022. DOI: 10.1103/PhysRevD.106.052009

[P321-2022] "Optimization of Graphene on D-Fiber Saturable Absorbers"

Londono-Giraldo, D. F.; Souza, E. A. T. de; **Fragnito, H. L.***

The graphene-light interaction in a waveguide can he optimized through the waveguide design. In the case of nonlinear optical devices, such as saturable absorbers, this optimization requires knowledge of the actual intensity that quantifies the nonlinear interaction with a waveguide mode. In this work we propose parameters that correctly quantify the strength of saturable absorption. We show that the graphene on D-fiber saturable absorber can be characterized through the absorption coefficient and a properly defined saturation power for each mode. We analyze the dependence of the graphene-light interaction on the geometrical parameters, chemical potential, number of graphene layers, and input power. The results show a wide variation of the graphene absorption with the design, which offers potential for polarizers with large polarization extinction ratios and saturable absorbers with low saturation powers. As a function of the number of layers, the interaction is maximized for five layers, and we predict a reverse saturable absorption effect for higher number of layers. The parameters introduced here to quantify the nonlinear graphene-light interaction can be applied to other waveguide structures and other 2D materials.

JOURNAL OF LIGHTWAVE TECHNOLOGY 40[18], 6249-6256, 2022. DOI: 10.1109/JLT.2022.3188216

[P322-2022] "Performance of optimal linear-response processes in driven Brownian motion far from equilibrium"

Kamizaki, L. P.*; Bonanca, M. V. S.*; Muniz, S. R.

Considering the paradigmatic driven Brownian motion, we perform extensive numerical analysis on the per-formance of optimal linear-response processes far from equilibrium. We focus on the overdamped regime where exact optimal processes are known analytically and most experiments operate. This allows us to compare the optimal processes obtained in linear response and address their relevance to experiments using realistic parameter values from experiments with optical tweezers. Our results help assess the accuracy of perturbative methods in calculating the irreversible work for cases where the exact solution might be difficult to access. For that, we present a performance metric comparing the approximate optimal solution to the exact one. Our main result is that optimal linear-response processes can perform surprisingly well, even far from where they were expected.

PHYSICAL REVIEW E 106[6], 064123, 2022. DOI: 10.1103/PhysRevE.106.064123

[P323-2022] "Physicochemical Properties of Ti3+ Self-Doped TiO2 Loaded on Recycled Fly-Ash Based Zeolites for Degradation of Methyl Orange"

Garcia, I. S.; Gomez, C. A. P.; Weber, M. H.; Gaona, I. M. S.; Martinez, C. P. C.; Zambrano, J. J. M.; Sarmiento, H. A. R.; Cagigas, J. A. M.; Avila, M. A.; **Rettori, C.***; Vargas, C. A. P.; Gomez, J. A. M.

The extensive production of coal fly ash by coal combustion is an issue of concern due to its environmental impact. TiO2-zeolite composites were synthesized, at low cost, using recycled coal fly ash from a local thermoelectric power plant to produce the zeolite using the hydrothermal method. TiO2 was loaded by means of the impregnation method using ethanol and titanium isopropoxide between 8.7 and 49.45 wt% TiO2. The samples were characterized by X-ray diffraction, Raman, electron spin resonance, high-resolution transmission electron microscopy, N-2 adsorption-desorption, doppler broadening of annihilation radiation, and diffuse reflectance techniques, and the photocatalytic activity of the composites was evaluated according to the degradation of methyl orange under UV light. The results show that TiO2 crystallizes in the anatase phase with a Ti3+ oxidation state, without post-treatment. TiO2 particles were located within the pores of the substrate and on its surface, increasing the surface area of the composites in comparison with that of the substrates. Samples with TiO2 at 8.7 and 25 wt% immobilized on hydroxysodalite show the highest degradation of methyl orange among all studied materials, including the commercial TiO2 Degussa P25 under UV light.

CONDENSED MATTER 7[4], 69, 2022. DOI: 10.3390/condmat7040069

[P324-2022] "Plastic deformation of superionic water ices"

Matusalem, .F.*; Rego, J. S.*; Koning, M. de*

Due to their potential role in the peculiar geophysical properties of the ice giants Neptune and Uranus, there has been a growing interest in superionic (SI) phases of water ice. So far, however, little attention has been given to their mechanical properties, even though plastic deformation processes in the interiors of planets are known to affect long-term processes, such as plate tectonics and mantle convection. Here, using density functional theory calculations and machine learning techniques, we assess the mechanical response of high-pressure/temperature solid phases of water in terms of their ideal shear strength (ISS) and dislocation behavior. The ISS results are well described by the renormalized Frenkel model of ideal strength and indicate that the SI ices are expected to be highly ductile. This is further supported by deep neural network molecular dynamics simulations for the behavior of lattice dislocations for the SI face-centered cubic (fcc) phase. Dislocation velocity data indicate effective shear viscosities that are orders of magnitude smaller than that of Earth's lower mantle, suggesting that the plastic flow of the internal icy layers in Neptune and Uranus may be significantly faster than previously foreseen.

PROCEEDINGS OF THE NATIONAL ACADEMY OF SCIENCES OF THE UNITED STATES OF AMERICA 119[45], e2203397119, 2022. DOI: 10.1073/pnas.2203397119

[P325-2022] "Production of K*(892)(0) and phi(1020) in pp and Pb-Pb collisions at root s(NN)=5.02 TeV"

Acharya, S.; Adamova, D.; **Chinellato, D. D.*; Guardiano, G. G.*; Jahnke, C.*; Lea, R.*; Takahashi, J.***; et al. ALICE Collaboration

The production of K *(892)(0) and phi(1020) mesons in proton--proton (pp) and lead-lead (Pb-Pb) collisions at root s(NN) = 5.02 TeV has been measured using the ALICE detector at the Large Hadron Collider (LHC). The transverse momentum (p(T)) distributions of K*(892)(0) and phi(1020) mesons have been measured at midrapidity (vertical bar y vertical bar < 0.5) up to p(T) = 20 GeV/c in inelastic pp collisions and for several Pb--Pb collision centralities. The collision centrality and collision energy dependence of the average transverse momenta agree with the radial flow scenario observed with stable hadrons, showing that the effect is stronger for more central collisions and higher collision energies. The K*(0)/K ratio is found to be suppressed in Pb-Pb collisions relative to pp collisions: this indicates a loss of the measured K *(892)(0) signal due to rescattering of its decay products in the hadronic phase. In contrast, for the longer-lived phi(1020) mesons, no such suppression is observed. The nuclear modification factors (R-AA) of K*(892) (0) and phi(1020) mesons are calculated using pp reference spectra at the same collision energy. In central Pb-Pb collisions for p(T) > 8 GeV/c, the R-AA values of K *(892)(0) and phi(1020) are below unity and observed to be similar to those of pions, kaons, and (anti)protons. The R-AA values at high pT (>8 GeV/c) for K*(892)0 and f(1020) mesons are in agreement within uncertainties for root s(NN) = 5.02 and 2.76 TeV.

PHYSICAL REVIEW C 106[3], 034907, 2022. DOI: 10.1103/PhysRevC.106.034907

[P326-2022] "Quantification of the Tissue Oxygenation Delay Induced by Breath-Holding in Patients with Carotid Atherosclerosis"

Quiroga, A.*; Novi, S.*; Martins, G.*; Bortoletto, L. F.*; Avelar, W.; Guillaumon, A. T.; Li, L. M.; Cendes, F.; **Mesquita, R. C.***

Carotid artery stenosis (CAS) is a common vascular disease with long-term consequences for the brain. Although CAS is strongly associated with impaired cerebral hemodynamics and neurodegeneration, the mechanisms underlying hemodynamic impairment in the microvasculature remain unknown. In this work, we employed functional near-infrared spectroscopy (fNIRS) to introduce a methodological approach for quantifying the temporal delay of the evoked hemodynamic response. The method was validated during a vasodilatory task (breath-holding) in 50 CAS patients and 20 controls. Our results suggest that the hemodynamic response to breath-holding can be delayed by up to 6 s in the most severe patients, a significant increase from the median 4 s measured for the control group (p = 0.01). In addition, the fraction of brain regions that responded to the task decreased as the CAS severity increased, from a median of 90% in controls to 73% in the most severe CAS group (p = 0.04). The presence of collateral circulation increases the response to breath-holding and decreases the average time delays across the brain, although the number of communicating arteries alone cannot predict these fNIRS-based hemodynamic variables (p > 0.09). Overall, this work proposes a method to quantitatively assess impaired cerebral hemodynamics in CAS patients.

METABOLITES 12[11], 1156, 2022. DOI: 10.3390/metabo12111156

[P327-2022] "Search for Higgs Boson Pair Production in the Four b Quark Final State in Proton-Proton Collisions at root s=13 TeV"

Tumasyan, A.; Adam, W.; **Chinellato, J. A.***; et al. CMS Collaboration

A search for pairs of Higgs bosons produced via gluon and vector boson fusion is presented, focusing on the four b quark final state. The data sample consists of proton-proton collisions at a center-of-mass energy of 13 TeV, collected with the CMS detector at the LHC, and corresponds to an integrated luminosity of 138 fb(-1). No deviation from the background--only hypothesis is observed. A 95% confidence level upper limit on the Higgs boson pair production cross section is observed at 3.9 times the standard model prediction for an expected value of 7.8. Constraints are also set on the modifiers of the Higgs field selfcoupling,.., and of the coupling of two Higgs bosons to two vector bosons,.2V. The observed (expected) allowed intervals at the 95% confidence level are -2.3 < kappa(lambda) < 9.4 (-5.0 < kappa(lambda) < 12.0) and -0.1 < kappa(2V) < 2.2 (-0.4 < kappa(2V) < 2.5). These are the most stringent observed constraints to date on the HH production cross section and on the kappa(2V) coupling.

PHYSICAL REVIEW LETTERS 129[8], 081802, 2022. DOI: 10.1103/PhysRevLett.129.081802

[P328-2022] "Shortcuts to Thermodynamic quasistaticity"

Soriani, A.*; Miranda, E.*; Deffner, S.; **Bonanca, M. V. S.***

The operation of near-term quantum technologies requires the development of feasible, implementable, and robust strategies of controlling complex many body systems. To this end, a variety of techniques, so-called "shortcuts to adiabaticity," have been developed. Many of these shortcuts have already been demonstrated to be powerful and implementable in distinct scenarios. Yet, it is often also desirable to have additional, approximate strategies available that are applicable to a large class of systems. Hence, in this Letter, we take inspiration from thermodynamics and propose to focus on the macrostate, rather than the microstate. Adiabatic dynamics can then be identified as such processes that preserve the equation of state, and systematic corrections are obtained from adiabatic perturbation theory. We demonstrate this approach by improving upon fast quasiadiabatic driving, and by applying the method to the quantum Ising chain in the transverse field.

PHYSICAL REVIEW LETTERS 129[18], 170602, 2022. DOI: 10.1103/PhysRevLett.129.170602

[P329-2022] "Size-Dependent Photobleaching Mechanism and Kinetics Induced by Nanosecond Laser Pulses in Colloidal Semiconductor Quantum Dots"

Santos, C. H. D. D. dos; Ferreira, D. L.; **Vale, B. R. C.***; Mourao, R. S.; Schiavon, M. A.; Vivas, M. G.

An experimental-theoretical approach is proposed to inves--tigate the size-dependent photobleaching of colloidal semiconductor quantum dots (QDs) excited by a nanosecond pulsed laser. In the experimental background, the ground-state absorption and photolumines-cence (PL) spectra of chemically prepared QDs are monitored over an excitation time at distinct laser irradiances. The magnitude of photobleaching in the QD solution is quantified by the decay rate of the PL signal as a function of the excitation time and the laser power. A theoretical spectroscopy model is then used to estimate the particle size distribution (PSD) in colloidal solution from the absorption data generated at different laser powers. The resulting evolution of the PSD of the QD ensemble under irradiation is analyzed in terms of classical crystallization theories dealing with the formation, growth, and dissolution of colloidal particles in a super-saturated medium.

The QD response to laser irradiation is also interpreted by a simple mechanical model that correlates the photoinduced hydrostatic strain at the solid/liquid interface and the predicted variation of the mean particle size. The reported experimental and theoretical methods are used to completely elucidate the basic physico-chemical processes responsible for the laser-induced photobleaching kinetics of glutathione--capped CdTe aqueous QDs with very small mean sizes. For this purpose, we synthesized a series of colloidal QD samples with mean particle diameters ranging from 1.95 to 2.68 nm. Our results indicate that a faster photobleaching rate occurs in QD samples with smaller sizes in which particle dissolution under laser irradiation is predominant. On the other hand, the photobleaching rate becomes slower in samples with larger dot sizes, possibly due to the formation of core/shell structures in solution via thermal degradation of thiol ligands either during the chemical synthesis or as a consequence of the subsequent interaction with the excitation laser.

LANGMUIR 38, 49, 15088-15105, 2022. DOI: 10.1021/acs.langmuir.2c02023

[P330-2022] "Strain Tuning in Graded SiGe on Insulator: Interplay between Local Concentration and Nonmonotonic Lattice Evolution after Ge Condensation"

Rodrigues-Junior, G.; Cavallo, F.; **Deneke, C.***; Malachias, A.

Germanium condensation has proven to be a reliable route for obtaining smoothly graded composition SiGe layers with good reproducibility and reduced defect density. The process is known as a crucial tool to induce well-defined strain on Si or SiGe layers with potential use in semiconductor devices. In this work, we show that starting from a low concentration Si0.92Ge0.08 layer grown on top of a crystalline Si(001) on SOI substrates, we can reach desirable concentration with a non-monotonic interplay on in-plane and out-of-plane strain. The Ge concentration is evaluated by a combination of ultralow energy secondary ion mass spectroscopy (ULE-SIMS) and synchrotron X-ray measurements (diffraction and reflectivity). After the evaluation of Ge content, the strain-sensitive process of rolling up tubes from the flat layers is used and combined with X-ray diffraction to provide a concise scenario of the strain evolution along an in-growth oxidation series, pointing out the conditions that maximize strain, as well as its fading, as the Ge content rises.

JOURNAL OF PHYSICAL CHEMISTRY C 126[50], 21368-21374, 2022. DOI: 10.1021/acs.jpcc.2c05702

[P331-2022] "Superficial Tale of Two Functional Groups: On the Surface Propensity of Aqueous Carboxylic Acids, Alkyl Amines, and Amino Acids"

Bjorneholm, O.; Ohrwall, G.; **Brito, A. N. de***; Agren, H.; Carravetta, V.

The gas–liquid interface of water is environmentally relevant due to the abundance of aqueous aerosol particles in the atmosphere. Aqueous aerosols often contain a significant fraction of organics. As aerosol particles are small, surface effects are substantial but not yet well understood. One starting point for studying the surface of aerosols is to investigate the surface of aqueous solutions. We review here studies of the surface composition of aqueous solutions using liquid-jet photoelectron spectroscopy in combination with theoretical simulations. Our focus is on model systems containing two functional groups, the carboxylic group and the amine group, which are both common in atmospheric organics. For alkanoic carboxylic acids and alkyl amines, we find that the surface propensity of such amphiphiles can be considered to be a balance between the hydrophilic interactions of the functional group and the hydrophobic interactions of the alkyl chain. For the same chain length, the neutral alkyl amine has a lower surface propensity than the neutral alkanoic carboxylic acid, whereas the surface propensity of the corresponding alkyl ammonium ion is higher than that of the alkanoic carboxylate ion. This different propensity leads to a pH-dependent surface composition which differs from the bulk, with the neutral forms having a much higher surface propensity than the charged ones. In aerosols, alkanoic carboxylic acids and alkyl amines are often found together. For such mixed systems, we find that the oppositely charged molecular ions form ion pairs at the surface. This cooperative behavior leads to a more organic--rich and hydrophobic surface than would be expected in a wide, environmentally relevant pH range. Amino acids contain a carboxylic and an amine group, and amino acids of biological origin are found in aerosols. Depending on the side group, we observe surface propensity ranging from surface-depleted to enriched by a factor of 10. Cysteine contains one more titratable group, which makes it exhibit more complex behavior, with some protonation states found only at the surface and not in the bulk. Moreover, the presence of molecular ions at the surface is seen to affect the distribution of inorganic ions. As the charge of the molecular ions changes with protonation, the effects on the inorganic ions also exhibit a pH dependence. Our results show that for these systems the surface composition differs from the bulk and changes with pH and that the results obtained for single-component solutions may be modified by ion–ion interactions in the case of mixed solutions.

ACCOUNTS OF CHEMICAL RESEARCH 55, 23, 3285-3293, 2022. DOI: 10.1021/acs.accounts.2c00494

[P332-2022] "The Role of the Extrafibrillar Volume on the Mechanical Properties of Molecular Models of Mineralized Bone Microfibrils"

Alcantara, A. C. S. de; **Felix, L. C.*; Galvao, D. S.***; Sollero, P.; Skaf, M. S.

Bones are responsible for body support, structure, motion, and several other functions that enable and facilitate life for many different animal species. They exhibit a complex network of distinct physical structures and mechanical properties, which ultimately depend on the fraction of their primary constituents at the molecular scale. Howe v e r , the relationship between structure and mechanical properties in bones are sti l l not fully understood . Here, we investigate structural and mechanical properties of all-atom bone molecular models composed of type-I collagen, hydroxyapatite (HA), and water by means of fully atomistic molecular dynamics simulations. Our models encompass an extrafibrillar volume (EFV) and consider mineral content in both the EFV and intrafibrillar volume (IFV), consistent with experimental observations. We investigate solvation structures and elastic properties of bone microfibri l models with different degrees of mineralization, ranging from highly mineralized to weakly mineralized and nonmineralized models. We find that the local tetrahedral order of water is lost in similar ways in the EFV and IFV regions for all HA containing models, as calcium and phosphate ions are strongly coordinated with water molecules. We also subject our models to tensile loads and analyze the spatial stress distribution over the nanostructure of the material . Our results show that both mineral and water contents accumulate significa n t l y higher stress levels, most notably in the EFV, thus revealing that this region, which has been only recently incorporated in all-atom molecular models, is fundamental for studying the mechanical properties of bones at the nanoscale. Furthermore, our results corroborate the well-established finding that high mineral content makes bone stiffer.

ACS BIOMATERIALS SCIENCE & ENGINEERING 2023, 9, 1, 230-245, 2022. DOI: 10.1021/acsbiomaterials.2c00728

[P333-2022] "Tiny spots to light the future: advances in synthesis, properties, and application of perovskite nanocrystals in solar cells"

Scalon, L.; Freitas, F. S.; **Marques, F. das C.*;** Nogueira, A. F.

Perovskites are in the hotspot of material science and technology. Outstanding properties have been discovered, fundamental mechanisms of defect formation and degradation elucidated, and applications in a wide variety of optoelectronic devices demonstrated. Advances through adjusting the bulk-perovskite composition, as well as the integration of layered and nanostructured perovskites in the devices, allowed improvement in performance and stability. Recently, efforts have been devoted to investigating the effects of quantum confinement in perovskite nanocrystals (PNCs) aiming to fabricate optoelectronic devices based solely on these nanoparticles. In general, the applications are focused on light-emitting diodes, especially because of the high color purity and high fluorescence quantum yield obtained in PNCs. Likewise, they present important characteristics featured for photovoltaic applications, highlighting the possibility of stabilizing photoactive phases that are unstable in their bulk analog, the fine control of the bandgap through size change, low defect density, and compatibility with large-scale deposition techniques. Despite the progress made in the last years towards the improvement in the performance and stability of PNCs-based solar cells, their efficiency is still much lower than that obtained with bulk perovskite, and discussions about upscaling of this technology are scarce. In light of this, we address in this review recent routes towards efficiency improvement and the up-scaling of PNC solar cells, emphasizing synthesis management and strategies for solar cell fabrication.

NANOSCALE 15[3], 907-941, 2022. DOI: 10.1039/d2nr05043a

[P334-2022] "Tip-Induced and Electrical Control of the Photoluminescence Yield of Monolayer WS2"

Roman, R. J. P.*; Bretel, R.; Pommier, D.; Lopez, L. E. P.; Lorchat, E.; Boer-Duchemin, E.; Dujardin, G.; Borisov, A. G.; **Zagonel, L. F.*;** Schull, G.; Berciaud, S.; Le Moal, E.

The photoluminescence (PL) of monolayer tungsten disulfide (WS2) is locally and electrically controlled using the nonplasmonic tip and tunneling current of a scanning tunneling microscope (STM). The spatial and spectral distribution of the emitted light is determined using an optical microscope. When the STM tip is engaged, short-range PL quenching due to near-field electromagnetic effects is present, independent of the sign and value of the bias voltage applied to the tip-sample tunneling junction. In addition, a bias-voltage-dependent long-range PL quenching is measured when the sample is positively biased. We explain these observations by considering the native n-doping of monolayer WS2 and the charge carrier density gradients induced by electron tunneling in micrometer-scale areas around the tip position. The combination of wide-field PL microscopy and charge carrier injection using an STM opens up new ways to explore the interplay between excitons and charge carriers in two-dimensional semiconductors.

NANO LETTERS 22[23], 9244-9251, 2022. DOI: 10.1021/acs.nanolett.2c02142

[P335-2022] "Two-Dimensional Multicomponent Quasicrystal as Bifunctional Electrocatalysts for Alkaline Oxygen and Hydrogen Evolution Reactions"

Mishra, S. S.; Kumbhakar, P .; Nellaiappan, S.; Katiyar, N. K.; **Tromer, R.*;** Wollner, C. F. F.; **Galvao, D. S.*;** Tiwary, C. S.; Ghosh, C.; Dasgupta, A.; Biswas, K.

The presence of weak interlayer interactions and in-plane covalent character in quasicrystals facilitate the synthesis of the two-dimensional multicomponent alloy by chemical exfoliation. The first large-scale formation of atomically thin 2D sheets by chemical exfoliation from the multicomponent Al-70Co10Fe5Ni10Cu5 decagonal quasicrystalline alloy is reported. The exfoliated ultrathin two-dimensional multicomponent alloy exhibits an excellent oxygen evolution reaction/hydrogen evolution reaction bifunctional catalytic activity in alkaline electrolyte, i.e., alkaline water splitting. The active surface area of the 2D sheets also provides a large number of active sites for the bifunctional catalysis of the oxygen and hydrogen evolution reactions. These 2D atomically thin sheets exhibit superior catalytic performance to their bulk counterparts. Molecular dynamics and density functional theory simulations of the 2D alloy support the experimental interpretation in terms of structural stability and catalytic properties. Synthesis of this type of new class 2D material provides a promising approach for the design and exploration of nonprecious transition metal-based electrocatalysts toward clean energy production.

ENERGY TECHNOLOGY, 2200860, 2022. DOI: 10.1002/ente.202200860

[P336-2022] "Unveiling the strain and structural ferroelectric phase transition induced by temperature in lead titanate perovskite modified with 40% of calcium"

Galao, L. R.*; Garcia, D.; Estrada, F. R.

Structurally correlated ferroelectric phase transitions induced by temperature are reported for the solid solution Pb0.6Ca0.4TiO3 compound. Such phase transitions were analyzed by considering different parameters, such as lattice parameters, microstrain, dielectric properties, and thermal analysis. Synchrotron x-ray diffraction and Rietveld refinement studies revealed a tetragonal symmetry from room temperature up to similar to;550 K and uniaxial microstrain from room temperature to similar to 400 K. The first thermally driven phase transition observed was from displacive ferroelectric tetragonal symmetry to another non-displacive tetragonal symmetry. The next phase transition was from the tetragonal to cubic. The electric permittivity as a function of temperature for frequency from 1 kHz to 1 MHz and the differential scanning calorimetry report features typical of ferroelectric-paraelectric phase transition only around 400 K, and no other abrupt change in properties is observed at 550 K, indicating the sequence of first- and then second-order phase transition.

JOURNAL OF APPLIED PHYSICS 132[24], 244101, 2022. DOI: 10.1063/5.0115572

[P337-2022] "Updating upsilon(3) lifetime from solar antineutrino spectra"

Picoreti, R.*; Pramanik, D.*; Holanda, P. C. de*; Peres, O. L. G.*

We study the production of antineutrinos from the solar neutrinos due to Majorana neutrino decays of neutrino to antineutrino. Using the antineutrino spectra from KamLAND and Borexino, we present the newest limits on the lifetime of. 3 in this scenario. We consider upsilon(3) -> (upsilon(1)) over bar + X and upsilon(3) -> (upsilon(2)) over bar + X channels assuming scalar or pseudoscalar interactions. For hierarchical mass-splittings, we obtain the limits tau(3)/m(3) >= 7 x 10(-5) s/eV and tau(3)/m(3) >= 1 x 10(- 5) s/eV for the two channels at 90% C.L. We found that the newest bound is five orders of magnitude better than the atmospheric and long-baseline bounds.

PHYSICAL REVIEW D 106[1], 2022. DOI: 10.1103/PhysRevD.106.015025

Eventos publicados 2022

[P338-2022] "Spin Chemistry Simulation via Hybrid-Quantum Machine Learning"

Brokowski, T. J.; Chowdhury, F. T.; Smith, L. D.; **Alvarez, P.*;** Sandeep, S.; Aiello, C. IEEE Comp Soc

The Radical Pair Mechanism, a process by which magnetic fields modulate the kinetics of chemical reactions by influencing spin dynamics, is thought to underlie a variety of biological mechanisms and is inherently both quantum and noisy. Model simulations with limited electron-nuclear interactions have been conducted on classical devices resulting in experimentally verified final state results, however these simulations become too complex to simulate as the systems scale in size. This motivates us to propound the simulation of the relevant spin dynamics in a noisy quantum device to probe the currently unexplored open quantum systems aspects of the radical pair mechanism and to provide a novel theoretical tool for us to be able to tackle bottlenecks in simulating larger and more physically relevant biological spin systems. We employ a hybrid quantum machine learning approach where we evaluate a parametrized quantum circuit representing the evolution of the system on the quantum device and then update the parameters according to our objective cost function on a classical computer using a gradient optimizer and a noisy gradient free (SPSA) optimizer. We show that a 3 qubit circuit with a series of parametrized rotation gates representing the Hyperfine and Zeeman interactions can be optimized, resulting in a circuit that evolves a singlet state under different magnetic field angles. Moreover, we show that the noisy gradient free optimizer is better suited for optimizing on a noisy quantum device. However, the precision in the quantum circuit outputs is only sub-par at present, leaving room for further improvements.

2022 IEEE INTERNATIONAL CONFERENCE ON QUANTUM COMPUTING AND ENGINEERING (QCE 2022), 867-868, 2022 DOI: 10.1109/QCE53715.2022.00147

Material editorial 2022

[M002-2022] "A narrow twist"

Alegre, T.*; Wiederhecker, G.*

One hundred years ago, in 1922, Leon Brillouin discovered the scattering of light by sound waves. Within an optical fibre, Brillouin scattering may be used to create narrow-linewidth filters and spectrometers. A twisted optical fibre is now used to reduce these linewidths by over an order of magnitude, down to the sub-MHz level.

NATURE PHOTONICS 16[7], 482-484, 2022. DOI: 10.1038/s41566-022-01029-4

***Autores da comunidade IFGW**
Fonte: Web of Science on-line (WOS)

Artigos publicados 2023

[P001-2023] "Boroxine benzaldehyde complex for pharmaceutical applications probed by electron interactions"

Pereira-da-Silva, J.; Nunes, A.; Mendes, M.; Rodrigues, R.; **Cornetta, L.***; Silva, F. F. da

Rationale 2,4,6-Tris(4-formylphenyl)boroxine (TFPB) is a substituted boroxine containing a benzaldehyde molecule bonded to each boron atom. Boroxine cages are an emerging class of functional nanostructures used in host-guest chemistry, and benzaldehyde is a potential radiosensitizer. Reactions initiated by low-energy electrons with such complexes may dictate and bring new fundamental knowledge for biomedical and pharmaceutical applications. Methods The electron ionization properties of TFPB are investigated using a gas-phase electron-molecule crossed beam apparatus coupled with a reflectron time-of-flight mass spectrometer in an orthogonal geometry. Ionization and threshold energies are experimentally determined by mass spectra acquisition as a function of the electron energy. Results The abundance of the molecular precursor cation in the mass spectrum at 70 eV is significantly lower than that of the most abundant fragment C7H5O+. Twenty-nine cationic fragments with relative intensities >2% are detected and identified. The appearance energies of six fragment cations are reported, and the experimental first ionization potential is found at 9.46 +/- 0.11 eV. Moreover, eight double cations are identified. The present results are supported by quantum chemical calculations based on bound state techniques, electron ionization models and thermodynamic thresholds. Conclusions According to these results, the TPFB properties may combine the potential radiosensitizer effect of benzaldehyde with the stability of the boroxine ring.

RAPID COMMUNICATIONS IN MASS SPECTROMETRY 37[1], e9418, 2023. DOI: 10.1002/rcm.9418

[P002-2023] "Consistent lensing and clustering in a low-S-8 Universe with BOSS, DES Year 3, HSC Year 1, and KiDS-1000"

Amon, A.; Robertson, N. C.; **Navarro-Alsina, A.***; et al.

We evaluate the consistency between lensing and clustering based on measurements from Baryon Oscillation Spectroscopic Survey combined with galaxy-galaxy lensing from Dark Energy Survey (DES) Year 3, Hyper Suprime-Cam Subaru Strategic Program (HSC) Year 1, and Kilo-Degree Survey (KiDS)-1000. We find good agreement between these lensing data sets. We model the observations using the DARK EMULATOR and fit the data at two fixed cosmologies: Planck (S-8 = 0.83), and a Lensing cosmology (S-8 = 0.76). For a joint analysis limited to large scales, we find that both cosmologies provide an acceptable fit to the data. Full utilization of the higher signal-to-noise small-scale measurements is hindered by uncertainty in the impact of baryon feedback and assembly bias, which we account for with a reasoned theoretical error budget. We incorporate a systematic inconsistency parameter for each redshift bin, A, that decouples the lensing and clustering. With a wide range of scales, we find different results for the consistency between the two cosmologies. Limiting the analysis to the bins for which the impact of the lens sample selection is expected to be minimal, for the Lensing cosmology, the measurements are consistent with A = 1; A = 0.91 +/- 0.04 (A = 0.97 +/- 0.06) using DES+KiDS (HSC). For the Planck case, we find a discrepancy: A = 0.79 +/- 0.03 (A = 0.84 +/- 0.05) using DES+KiDS (HSC). We demonstrate that a kinematic Sunyaev-Zeldovich-based estimate for baryonic effects alleviates some of the discrepancy in the Planck cosmology. This analysis demonstrates the statistical power of small-scale measurements; however, caution is still warranted given modelling uncertainties and foreground sample selection effects.

MONTHLY NOTICES OF THE ROYAL ASTRONOMICAL SOCIETY 518[1], 477-503, 2023. DOI: 10.1093/mnras/stac2938

[P003-2023] "Effect of viscosity and colloidal stability on the magnetic hyperthermia of petroleum-based nanofluids"

Pinheiro, I. F.; **Brollo, M. E. F.*; B**assani, G. S.; Varet, G.; Merino-Garcia, D.; Guersoni, V. C. B.; **Knobel, M.*;** Bannwart, A. C.; **Muraca, D.*;** van der Geest, C.

Magnetic Hyperthermia (MH) is the increase in temperature of a colloid composed of suspended magnetic nanoparticles (NP), which occurs when subjected to high frequency alternate magnetic fields (AMF). When well controlled, this phenomenon has shown great potential for industrial and medical applications. In this work, we investigate the effect of important variables such as viscosity, NP concentration, and colloidal stability to maximize the heat transferred from the AMF to the colloid. Iron oxide nanoparticles with core size of 9 nm (a-= 0.3) were used in the colloid, forming a stable system for six days in diesel, for both NP concentrations tested (0.5 and 1 wt.%). The NP and Diesel mixture was then added to two different viscosity crude oils (Heavy and Waxy). The maximum AT achieved in two minutes with 0.5 wt.% NP (770 kHz and 28 kA/m) was 59 degrees C for diesel, 57 degrees C for heavy crude oil, and 43 degrees C for waxy crude oil, respectively, with up to 95 degrees C for 1.0 wt.% NP dispersed in diesel. It was therefore possible to observe a clear increase in the system's temperature by applying MH in high viscous liquids (> 1000 mPa.s) with superparamagnetic nanoparticles.

FUEL 331, 125810, parte 2, 2023. DOI: 10.1016/j.fuel.2022.125810

[P004-2023] "Evidence for Dyakonov-Perel spin relaxation in Gd3+ doped YFe2Zn20"

Cabrera-Baez, M.; Padron-Hernandez, E.; Avila, M. A.; **Rettori, C.***

We report on the magnetic, thermodynamic, and electronic properties of the Gd-doped nearly ferromagnetic Fermi liquid (NFFL) system YFe2Zn20 by means of dc magnetic susceptibility, specific heat, and electron spin resonance (ESR) measurements. As Gd is incorporated (Y1-xGdxFe2Zn20; x = 0.005, 0.01, and 0.05), the magnetization measurements present evidence of ferromagnetic correlations with unusual results in temperaturedependent ESR experiments for all samples. Strong evidence of an induced conduction ESR (CESR) is found due to the presence of Gd3+ ions for all of the doped samples. The usual local magnetic moment resonance associated with Gd3+ 4 f localized electrons were only present for x = 0.05, coexisting with the CESR. Although YFe2Zn20 is a NFFL, no CESR was detected for the undoped sample, demonstrating the role of Gd3+ as a CESR activator. These results are discussed in terms of a highly polarized, enhanced Pauli paramagnetism of d-type electrons and a Dyakonov-Perel-like relaxation mechanism involving spin-flip due to magnetic impurities.

PHYSICAL REVIEW B 107[1], 014401, 2023. DOI: 10.1103/PhysRevB.107.014401

[P005-2023] "Mechanical properties of tetragraphene single-layer: A molecular dynamics study"

Brandao, W. H. S.; Aguiar, A. L.; **Fonseca, A. F.*; Galvao, D. S.***; Sousa, J. M. De

Recently, a quasi-2D semiconductor carbon allotrope called tetragraphene (TG), was proposed. TG is composed of square and hexagonal rings. Some of the TG properties were predicted based on first-principles simulations, but a comprehensive study of its mechanical behavior at different temperatures is still lacking. In this work, using fully atomistic reactive molecular dynamics simulations, we investigated TG mechanical properties under tensile strain, from the linear regime up to the complete fracture. One interesting result is that TG experiences a transition from crystalline to an amorphous structure induced by temperature and/or tension application. At room temperature, the critical strains along the TG two unit-cell directions are 38% and 30%, which is higher than the corresponding ones for graphene and penta-graphene, while its elastic modulus and ultimate tensile strength values are smaller.

MECHANICS OF MATERIALS 176, 104503, 2023. DOI: 10.1016/j.mechmat.2022.104503

[P006-2023] "Physical and digital phantoms for 2D and 3D x-ray breast imaging: Review on the state-of-the-art and future prospects"

Sarno, A.; Valero, C.; Tucciariello, R. M.; Dukov, N.; Costa, P. R.; **Tomal, A.***

Breast phantoms are a fundamental asset both in routine quality assurance programs and for comparing scanner performance in 2D and 3D x-ray breast imaging. They also play an essential role in the optimization of imaging systems and for testing new technologies before their introduction in the clinical practice. The ideal phantom must reflect and mimic the organ anatomy and pathologies, including details such as simulated tumor masses or microcalcifications. They can also be designed to evaluate a particular technical specification of the detector or of the imaging setup, such as noise or spatial resolution. The introduction of digital breast tomosynthesis (DBT) and computed tomography dedicated to the breast (BCT) in the clinical practice allowed to acquire 3D breast images with relatively high contrast and spatial resolution. The introduction of these innovative technologies encouraged the development of new phantoms for quality assurance and systems comparisons; on the other hand, 3D images of the breasts acquired with DBT and BCT apparatuses along with innovative and low-cost additive manufacturing technologies have been the basis for the development of a new class of digital and physical anthropomorphic breast phantoms. In these cases, the realism has been demonstrated to be fundamental in overtaking the limits of conventional phantoms used in digital mammography (DM) quality assurance programs. This work aims at reviewing the conventional phantoms adopted for testing and optimizing DM, DBT and BCT systems and to furnish a critical insight in emerging physical and digital breast phantoms. The limitations of conventional phantoms will be outlined, also regarding the needs of comparing apparatuses which adopt a compressed breast geometry to modern BCT ones, with pendant uncompressed breast geometry.

RADIATION PHYSICS AND CHEMISTRY 204, 110715, 2023. DOI: 10.1016/j.radphyschem.2022.110715

[P007-2023] "Prediction of DNA rejoining kinetics and cell survival after proton irradiation for V79 cells using Geant4--DNA"

Sakata, D.; Hirayama, R.; **Bernal, M. A.*;** et al.

Purpose: Track structure Monte Carlo (MC) codes have achieved successful outcomes in the quantitative investigation of radiation-induced initial DNA damage. The aim of the present study is to extend a Geant4-DNA radiobiological application by incorporating a feature allowing for the prediction of DNA rejoining kinetics and corresponding

cell surviving fraction along time after irradiation, for a Chinese hamster V79 cell line, which is one of the most popular and widely investigated cell lines in radiobiology. Methods: We implemented the Two-Lesion Kinetics (TLK) model, originally proposed by Stewart, which allows for simulations to calculate residual DNA damage and surviving fraction along time via the number of initial DNA damage and its complexity as inputs. Results: By optimizing the model parameters of the TLK model in accordance to the experimental data on V79, we were able to predict both DNA rejoining kinetics at low linear energy transfers (LET) and cell surviving fraction.Conclusion: This is the first study to demonstrate the implementation of both the cell surviving fraction and the DNA rejoining kinetics with the estimated initial DNA damage, in a realistic cell geometrical model simulated by full track structure MC simulations at DNA level and for various LET. These simulation and model make the link between mechanistic physical/chemical damage processes and these two specific biological endpoints.

PHYSICA MEDICA-EUROPEAN JOURNAL OF MEDICAL PHYSICS 105, 102508, 2023. DOI: 10.1016/j.ejmp.2022.11.012

[P008-2023] "X-ray photoelectron diffraction study of the approximant Al5Co2(001) quasicrystal"

Senna Junior, L. de; Pancotti, A.; Kilian, A. S.; **Siervo, A. de*;** Diehl, R. D.; Weerd, M. C. de; Ledieu, J.; Gaudry, E.; Fournee, V.; Abreu, G. J. P.

The intermetallic Al5Co2 is defined as a structurally complex material and is considered a low-order quasicrystalline approximant. A single crystal of Al5Co2(001) was obtained by the Czochralski method. The sample was characterized by X-ray photoelectron spectroscopy (XPS), low-energy electron diffraction (LEED), and X-ray photoelectron diffraction (PED). The surface composition was also analyzed by XPS, indicating only Al and Co compounds. In the current research, the crystal structure was qualitatively analyzed using the LEED patterns for different incident beam energies indicating a (1 x 1) termination, also in accordance with some literature works. The structure study was performed by applying the standard software MSCD and showed a (1 x 1) pattern. In addition, four different termination models for this termination were tested. The reliability factor indicated that the best termination belongs to the Al-rich surface layer.

PHYSICAL CHEMISTRY CHEMICAL PHYSICS 25[4], 3387-3394, 2023. DOI: 10.1039/d2cp04891d

***Autores da comunidade IFGW**
Fonte: Web of Science on-line (WOS)

Defesas de Dissertações do IFGW

[D001-2023] "Crescimento por laser pulsado e caracterização de filmes finos de YBa2Cu3O7´δ e Sr2IrO4"
Aluno: Karine Silva Alcantara
Orientador: Prof. Dr. Pedro Schio de Noronha Muniz
Data: 16/02/2023

Defesas de Teses do IFGW

[T001-2023] "Técnicas de Raios X Aplicadas ao Estudo de Supercondutores em Pressões Extremas"
Aluno: Lucas Henrique Francisco
Orientador: Prof. Dr. Narcizo Marques de Souza Neto
Data: 03/02/2023

[T002-2023] "Física de Neutrinos na Nova Era da Cosmologia"
Aluno: Anderson Luiz Brandão de Souza
Orientador: Profa. Dra. Flávia Sobreira
Data: 03/02/2023

Fonte: Portal IFGW/Pós-graduação - Agenda de Colóquios, Defesas e Seminários.
Disponível em: http://portal.ifi.unicamp.br/pos-graduacao

Observação: Não ocorreram neste período defesas de teses e dissertações, com orientadores ou banca do IFGW, do Programa de Pós-Graduação Multiunidades em Ensino de Ciências e Matemática – Mestrado e Doutorado (PECIM) da Unicamp.

Fonte: Página do PECIM
Disponível em: https://www.pecim.unicamp.br/bancas

Abstracta

Instituto de Física
Diretor: Profa. Dra. Mônica Alonso Cotta
Diretora Associada: Prof. Dr. Marcos Cesar de Oliveira
Universidade Estadual de Campinas - UNICAMP
Cidade Universitária Zeferino Vaz
13083-859 - Campinas - SP - Brasil
e-mail: secdir@ifi.unicamp.br
Fone: +55 19 3521-5300

Publicação

Biblioteca do Instituto de Física Gleb Wataghin
http://portal.ifi.unicamp.br/biblioteca
Instagram: @bif.unicamp
Telegram: t.m/bifunicamp

Diretora Técnica: Sandra Maria Carlos Cartaxo
Coordenadora da Comissão de Biblioteca: Profa. Dra. Arlene Cristina Aguilar

Elaboração:
Maria Graciele Trevisan (Bibliotecária)
contato: infobif@ifi.unicamp.br